Investigation of the Structure and Magnetism in Lanthanide β-Triketonate Tetranuclear Assemblies

Brodie L. Reid,[a] Robert C. Woodward,[b] Rebecca O. Fuller,[c] Alexandre N. Sobolev,[d] Brian W. Skelton,[d] Mark I. Ogden,*[a] and Massimiliano Massi*[a]

[a] *Department of Chemistry, and Nanochemistry Research Institute, Curtin University, Kent Street, Bentley 6102 WA, Australia.*

[b] *School of Physics, The University of Western Australia, Crawley, Western Australia 6009, Australia*

[c] *Chemistry M310, School of Chemistry and Biochemistry, University of Western Australia, Crawley, Western Australia 6009, Australia*

[d] *Centre for Microscopy, Characterisation and Analysis, University of Western Australia, Crawley 6009 WA, Australia.*

Corresponding Authors

*E-mail: m.massi@curtin.edu.au; m.ogden@curtin.edu.au.

Keywords: lanthanides, magnetism, triketonates, diketonates, assemblies.

Abstract

The preparation of discrete tetranuclear lanthanide/alkali metal (Ae) assemblies bearing a tribenzoylmethane ligand (**L**H) is discussed. These assemblies have the general formula $[Ln(Ae{\cdot}HOEt)(\mathbf{L})_4]_2$, where Ln^{3+} = Gd^{3+}, Tb^{3+}, Dy^{3+}, Ho^{3+} and Ae^{+} = Na^{+}, K^{+}, Rb^{+}. The coordination geometries of the lanthanide species were analysed and compared, revealing a trend between an eight-coordinate square antiprism and triangular dodecahedron dependent on the nature of lanthanide, alkali metal, and lattice solvent. The potassium-containing analogues were also analysed for their magnetic susceptibility.

Introduction

Coordination complexes of the trivalent lanthanide ions have been extensively investigated due to the intrinsic magnetic and optical properties arising from the 4*f*-electrons. The interest is well justified by the many technological applications found by lanthanide-containing compounds, spanning optical displays,[1–3] telecommunication devices,[4,5] and magnets[6] as well as diagnostic and therapeutic medicinal agents.[7,8] In this field, the β-diketonate class of ligands is certainly ubiquitous, which is due to their ability to efficiently bind oxophilic trivalent lanthanide ions forming relatively stable complexes. β-Diketonate ligands are also known to be able to stabilise various structural motifs when binding to lanthanide cations, ranging from mononuclear complexes to extended oxo/hydroxo clusters obtained *via* the established "controlled hydrolysis" synthesis.[9–12]

Given the enormous research effort focussed on lanthanide β-diketonate complexes, it is rather surprising that the analogous β-triketonate complexes have received very scarce attention.[13–15] This is even more remarkable considering that β-triketonate ligands are synthetically accessible *via* facile Claisen-type condensations from β-diketonate ligands.

We have recently initiated an investigation focussed on evaluating the coordination chemistry and optical properties of lanthanide β-triketonate complexes using the tribenzoylmethanide ligand. Our studies revealed the formation of discrete Ln^{3+}/Ae^{+} tetranuclear assemblies of the general formula $[Ln(Ae{\cdot}HOEt)(\mathbf{L})_4]_2$, where Ln^{3+} = Eu^{3+}, Er^{3+}, and Yb^{3+}; and Ae^{+} = Na^{+}, K^{+}, and Rb^{+}.[16,17] This family of compounds proved to be remarkably robust to variations of the identity of the lanthanide as well as the alkali metal cations. Our work was initially focussed on the investigation of the photophysical properties of these assemblies, thus using red emitting

Eu^{3+} cations and near-infrared emitting Er^{3+} and Yb^{3+} cations. We have now continued our research effort to extend the family of these assemblies including the lanthanide ions Gd^{3+}, Tb^{3+}, Dy^{3+}, and Ho^{3+}. Furthermore, we have started a preliminary investigation of their magnetic properties. Molecular magnets being developed around single lanthanide nuclei with large ground spin states use the inherent magnetic anisotropy and ligand field symmetry to produce the desired slow magnetic relaxation. More recently, dinuclear lanthanide complexes have also been shown to exhibit desirable properties. However unlike their mononuclear counterparts, these complexes tend to have strong magnetic exchange interactions through a radical bridging atom.[18,19]

Results and Discussion

Synthesis

The tribenzoylmethane ligand **L**H was synthesized according to our previously reported procedure,[16] in which dibenzoylmethane was reacted with benzoyl chloride and NaH in diethyl ether. The preparation of the Ln^{3+}/Ae^{+} tetranuclear assemblies, $[Ln(Ae{\cdot}HOEt)(\mathbf{L})_4]_2$ (in this case Ln^{3+} = Gd^{3+}, Tb^{3+}, Dy^{3+}, Ho^{3+}; Ae^{+} = K^{+}, Rb^{+}), was analogous to our previously reported procedure,[16,17] whereby four equivalents of **L**H and AeOH were reacted with one equivalent of hydrated $LnCl_3$ in ethanol (Figure 1). The synthesis of the $[Tb(Na{\cdot}HOEt)(\mathbf{L})_4]_2$ tetranuclear assembly is also reported herein, using NaOH base. The targeted assemblies were in general characterised by means of IR spectroscopy and elemental analysis. In particular, the latter proved in some cases difficult to obtain, as the assemblies have the tendency to often co-crystallise as solvates containing various degrees of lattice solvent molecules. This characteristic is analogous to the previously reported assemblies of Eu^{3+}, Er^{3+}, and Yb^{3+}. While the preparation of these assemblies was attempted with all the lanthanide ions, their isolation with elements lighter than Eu^{3+} has proven to be unsuccessful to date.

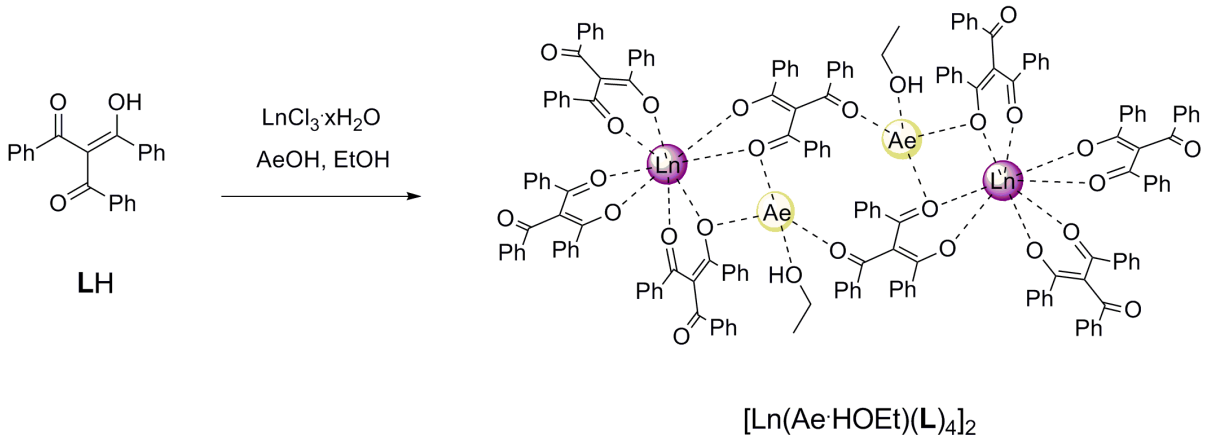

Figure 1 - Synthetic pathway to lanthanide assemblies bearing β-triketonate ligands. Ln^{3+} = Gd^{3+}, Tb^{3+}, Dy^{3+}, Ho^{3+}; Ae^{+} = K^{+}, Rb^{+}.

X-ray diffraction

As found previously,[16,17] the tetranuclear $[Ln(Ae{\cdot}HOEt)(\mathbf{L})_4]_2$ assemblies are neutral discrete species whereby both Ln^{3+} cations are eight-coordinate by four bis-chelating β-triketonate ligands. A dimer is formed through the coordination of an alkali metal through the third keto arm of one β-triketonate molecule (see Figure 2 for $[Tb(K{\cdot}HOEt)(\mathbf{L})_4]_2$ structure; see Supporting Information for all other structures).

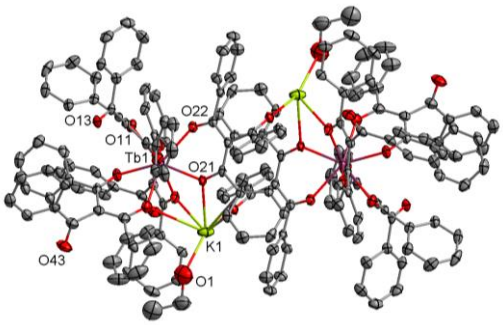

Figure 2 – Molecular plot of the $[Tb(K{\cdot}HOEt)(\mathbf{L})_4]_2$ assembly with displacement ellipsoids at the 50% probability level.

Although each of the successfully isolated $[Ln(Ae{\cdot}HOEt)(\mathbf{L})_4]_2$ assemblies are analogous in structure, it was determined that, in addition to unsolvated structures, the assemblies can also

crystallise as a different solvate, namely, $[Ln(Ae{\cdot}HOEt)(\mathbf{L})_4]_2{\cdot}2(EtOH)$. In fact, for the $[Dy(K{\cdot}HOEt)(\mathbf{L})_4]_2$ assembly, both unsolvated and solvated structures were identified by single crystal X-ray diffraction from the same crystallisation vial. This behaviour was also previously observed in the case of the Yb^{3+}/K^+ assembly.[16,17] Table 1 describes each of the assemblies presented as their crystallised species, as well as an abbreviation to describe each assembly, $\{Ln_2Ae_2\}$, which will be used to denote the assemblies throughout the manuscript. It is interesting to note that the assemblies are essentially isomorphous when their structures possess the same degree of solvation, irrespective of the identity of the lanthanide and/or alkali metal cations.

Table 1 - Tetranuclear assemblies sorted by their isomorphous crystallised structures.

Formulation	**$\{Ln_2Ae_2\}$ Assemblies**
$[Ln(Na{\cdot}HOEt)(\mathbf{L})_4]_2$	$\{Tb_2Na_2\}$
$[Ln(K/Rb{\cdot}HOEt)(\mathbf{L})_4]_2$	$\{Tb_2K_2\}$,$\{Dy_2K_2\}$, $\{Ho_2K_2\}$
$[Ln(Ae{\cdot}HOEt)(\mathbf{L})_4]_2{\cdot}2EtOH$	$\{Tb_2Rb_2\}$, $\{Gd_2K_2\}$, $\{Gd_2Rb_2\}$, $\{Dy_2K_2\}$, $\{Dy_2Rb_2\}$, $\{Ho_2Rb_2\}$

Selected distances are given in Table 2 for each assembly, including average Ln-O distances, and Ln···Ln distances. The average Ln-O distance for all assemblies decreases from Tb^{3+} (~2.36 Å) to Ho^{3+} (~2.33 Å), consistent with considerations based on the lanthanide contraction. The Ln···Ln distance in each of the assemblies were found to be affected by the lanthanide contraction, but also the presence (or absence) of co-crystallised solvent molecules and the identity of the alkali metal. The lanthanide contraction gives rise to a general decrease in Ln···Ln distance, within crystal formulation.

This trend is only comparable within each formulation, and thus the position of the alkali metal-bound ethanol molecule has a profound effect on the packing of the tetranuclear assemblies and the Ln···Ln distance. Furthermore, the presence of the K^+ or Rb^+ alkali metal presents some anomalies in the lanthanide contraction trend within each formulation, which is not unexpected due to the larger size of the Rb^+ ion compared to the K^+ ion.

Table 2 - Selected distances (Å) between the two lanthanide cations (Ln···Ln) within the tetranuclear assemblies, and average Ln-O bond distances within the first coordination sphere. Structures are grouped by their formulation.

Formulation	Assembly	Ln···Ln	Ave. Ln-O
$[Ln(Na{\cdot}HOEt)(\mathbf{L})_4]_2$	$\{Tb_2Na_2\}$	8.9547(4)	2.354
$[Ln(K/Rb{\cdot}HOEt)(\mathbf{L})_4]_2$	$\{Tb_2K_2\}$	8.8380(5)	2.358
	$\{Dy_2K_2\}$	8.8207(4)	2.344
	$\{Ho_2K_2\}$	8.8033(2)	2.332
$[Ln(Ae{\cdot}HOEt)(\mathbf{L})_4]_2{\cdot}2EtOH$	$\{Tb_2Rb_2\}$	8.9374(1)	2.357
	$\{Gd_2K_2\}$	8.9664(5)	2.369
	$\{Gd_2Rb_2\}$	8.9514(5)	2.372
	$\{Dy_2K_2\}$	8.9461(4)	2.344
	$\{Dy_2Rb_2\}$	8.9214(2)	2.343
	$\{Ho_2Rb_2\}$	8.9076(4)	2.330

The coordination geometries of all species were assessed using Shape Version 2.1 software[20,21] and were found have continuous shape measures (CShM) best describing a square antiprism or a triangular dodecahedron polyhedron (see Supporting Information for CShM values).

These CShM values were plotted on a shape map together with the CShM values of our previously reported assemblies[17] (Figure 3, for CShM values of our previously reported assemblies - see the literature[17]). The shape map illustrates clearly that a variety of CShM clusters emerges. Interestingly, it was noted that the presence (or absence) of the lattice solvent molecules and the identity of the Ae^+ cation have an influence on the specific geometry of the coordination environment around the lanthanide centre. These clusters correspond to the assemblies within the different crystallised formulations such as those described previously.

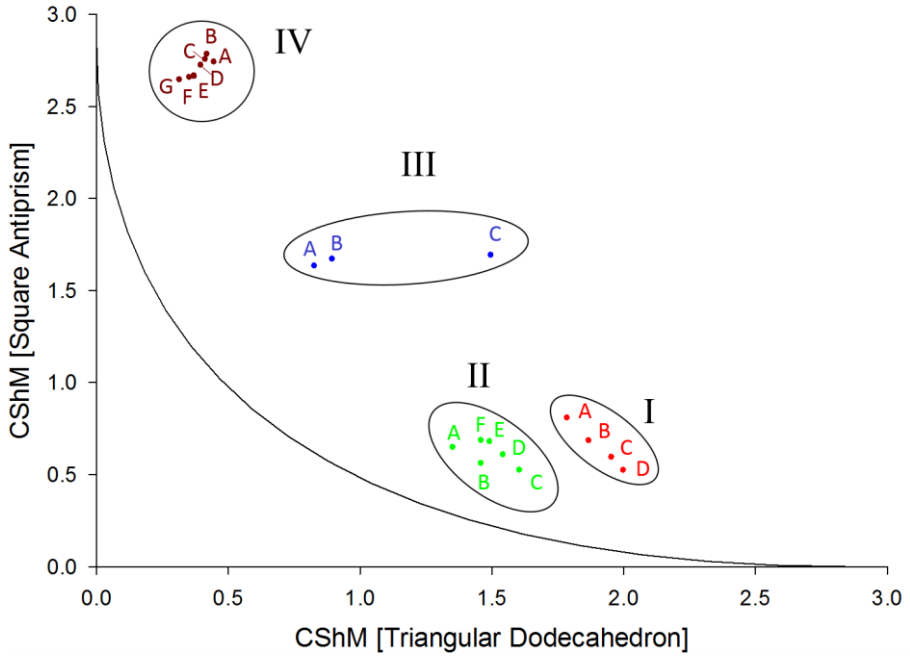

[Ln(Na·HOEt)(**L**)$_4$]$_2$ (**I**)	[Ln(K/Rb·HOEt)(**L**)$_4$]$_2$ (**II**)	[Ln(Ae·HOEt)(**L**)$_4$]$_2$·2(H$_2$O)(EtOH) (**III**)	[Ln(Ae·HOEt)(**L**)$_4$]$_2$·2(EtOH) (**IV**)
A: *{Eu$_2$Na$_2$}*	A: *{Er$_2$Rb$_2$}*	A:*{Yb$_2$K$_2$}*	A: *{Eu$_2$K$_2$}*
B: **{Tb$_2$Na$_2$}**	B: *{Yb$_2$Rb$_2$}*	B: *{Er$_2$K$_2$}*	B:*{Eu$_2$Rb$_2$}*, **{Gd$_2$K$_2$}**
C: *{Er$_2$Na$_2$}*	C: *{Yb$_2$K$_2$}*	C: *{EuK-BuOH}*	C: **{Gd$_2$Rb$_2$}**
D: *{Yb$_2$Na$_2$}*	D: **{Ho$_2$K$_2$}**		D: **{Dy$_2$K$_2$}**
	E: **{Tb$_2$K$_2$}**		E: **{Tb$_2$Rb$_2$}**
	F: **{Dy$_2$K$_2$}**		F: **{Dy$_2$Rb$_2$}**
			G: **{Ho$_2$Rb$_2$}**

Figure 3 - Top: Shape map presenting the CShM of the 21 lanthanide/alkali metal assemblies presented previously and herein, against the reference square antiprism and triangular dodecahedron polyhedra. The black trace represents the lowest energy interconversion pathway (LEIP) between the two reference polyhedra. Classes of assemblies are circled and the class number printed alongside. Bottom: The legend is shown in the table. Bolded formulations are reported in this manuscript, whereas italicised formulations have been reported elsewhere.[16,17]

It is interesting to note that the major factor contributing to the coordination geometry seems to be the degree of solvation and nature of the lattice solvent molecules. The

[Ln(Na·HOEt)**(L)**$_4$]$_2$ (**I**) species have a coordination geometry that is closest to a square antiprism, irrespective of the lanthanide cation. The deviation from the lowest energy interconversion pathway (LEIP, black line in Figure 4) increases from the smaller Yb^{3+} to the larger Eu^{3+} indicating a distortion away from the regular polyhedra with increasing lanthanide size.

From this arrangement, a slight distortion is observed for the [Ln(K/Rb·HOEt)**(L)**$_4$]$_2$ (**II**) structures, however the coordination sphere is again best described by a square antiprism geometry. The deviation from the LEIP follows the same trend as the [Ln(Na·HOEt)**(L)**$_4$]$_2$ structures which increases with increasing lanthanide size, from {Yb_2K_2} to {Tb_2K_2}.

Further distortion is evident for the previously reported [Ln(Ae·HOEt)**(L)**$_4$]$_2$·2(H_2O)(EtOH) (**III**) structures.[17] The deviation trend is again consistent from {Yb_2K_2} to {Er_2K_2}.

Lastly, better described as a triangular dodecahedron, lie the [Ln(Ae·HOEt)**(L)**$_4$]$_2$·2(EtOH) (**IV**) assemblies with two lattice ethanol molecules. Again, the deviation from the LEIP increases with increasing lanthanide size, from {Ho_2Rb_2} to {Eu_2K_2}. In the solvated (**IV**) series, the presence of K^+ or Rb^+ appears to affect the deviation from regular polyhedra to a lesser extent. This observation is most likely due to the fact that the investigated structures now include larger lanthanides, whose coordination geometry is less affected by the size of the alkali metal.

Static Magnetic Properties

Static magnetic properties for the K^+ containing assemblies were investigated (Figure 4).

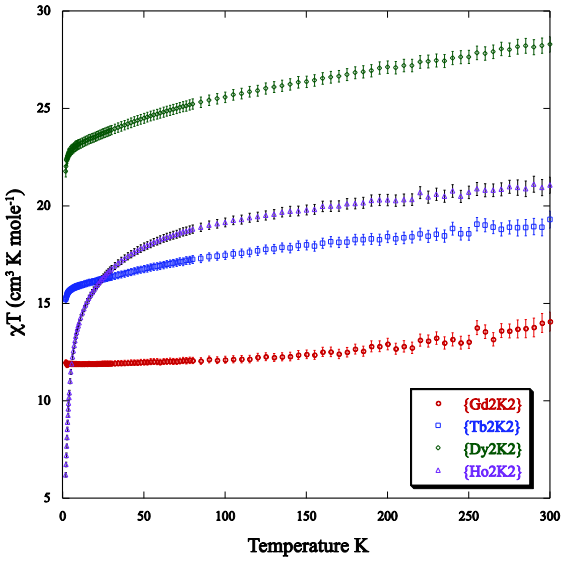

Figure 4 – The temperature dependent $\chi_M T$ profiles in a 100 Oe field for the $\{Gd_2K_2\}$ (red), $\{Dy_2K_2\}$ (green), $\{Tb_2K_2\}$ (blue) and $\{Ho_2K_2\}$ (pink) assemblies.

The $\chi_M T$ product for $\{Gd_2K_2\}$ assembly decreases slightly from the room temperature value of 14.1 cm^3 K mol^{-1} to 11.9 cm^3 K mol^{-1} at 20 K. This value is slightly lower than the expected 15.7 cm^3 K mol^{-1} spin only value for two uncoupled Gd ions (S=7/2, $^8S_{7/2}$, g=2). The susceptibility product then remains relatively constant below 20K. The room temperature value of $\chi_M T$ 28.3 cm^3 K mol^{-1} found for the $\{Dy_2K_2\}$ cluster is within experimental error of the expected values of 28.2 cm^3 K mol^{-1} for two uncoupled Dy^{3+} ions (S=5/2, L=5, $^6H_{15/2}$). However $\chi_M T$ for the $\{Tb_2K_2\}$ (20.1 cm^3 K mol^{-1}) and $\{Ho_2K_2\}$ (21.1 cm^3 K mol^{-1}) complexes are lower than the expected values for two uncoupled Tb^{3+} S=3, L=3, $^7F_6$ 23.6 cm^3 K mol^{-1}) or Ho^{3+} (S=2, L=4, $^5I_{15/2}$ 28 cm^3 K mol^{-1}) ions. As temperature is lowered, $\chi_M T$ decreases gradually. This decrease is likely the result of the depopulation of the excited Stark levels and the exchange interaction between atoms.[22] At lower temperatures this decrease is more rapid, likely the result of the crystal field effect[23] or the presence of weak antiferromagnetic interactions between the atoms.

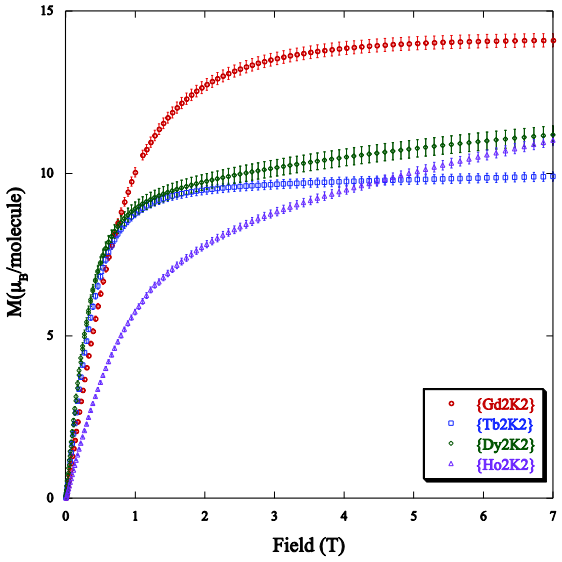

Figure 5 – Field dependent M vs H/T plots at 2 K for the $\{Gd_2K_2\}$ (red), $\{Dy_2K_2\}$ (green), $\{Tb_2K_2\}$ (blue) and $\{Ho_2K_2\}$ (pink) assemblies.

The field dependence of the magnetisation for all complexes exhibits a fast increase in weak fields. While when larger fields are applied the magnetisation only increases slowly for the $\{Gd_2K_2\}$, $\{Dy_2K_2\}$ and $\{Ho_2K_2\}$. For $\{Dy_2K_2\}$ and $\{Ho_2K_2\}$ the slow rise is likely due to the magnetic anisotropy associated with the Dy and Ho atoms. Further increasing the field results in the saturation of the magnetisation for both the $\{Gd_2K_2\}$ and $\{Dy_2K_2\}$. For $\{Dy_2K_2\}$ value deviates significantly from the theoretical saturation. The magnetisation continues to increase for $\{Tb_2K_2\}$ and $\{Ho_2K_2\}$ complexes at 7 T. The smaller than expected values measured at 7 T supports the occurrence of both magnetic anisotropy and ligand field induced splitting of the Stark Levels.[22]

Conclusion

The sequence of tetranuclear Ln^{3+}/Ae^{+} clusters reported here confirms that the tribenzoylmethane ligand can support these clusters for the lanthanide cations ranging from Eu^{3+} to Yb^{3+}, with efforts to obtain crystalline products for the lighter lanthanides being unsuccessful to date. The different solvates obtained are found to have a significant influence on the coordination sphere geometry of the lanthanide centres, but the specific solvate obtained is not strongly influenced by the nature and size of the lanthanide cations, as illustrated by the

isolation of two different Dy^{3+}/K^{+} solvates from one flask. The magnetic properties of the complexes reported here are not entirely as expected, especially in considering the values of $\chi_M T$ for some of the isolated assemblies. Deviations observed are tentatively ascribed to the presence of various solvates, and crystal field effects, in the bulk samples.

Experimental Section

General procedures

All reagents and solvents were purchased from chemical suppliers and used as received without further purification. The ligand, 2-benzoyl-1,3-diphenyl-1,3-propandione (**L**H), was prepared as we have previously reported.[16] Hydrated $LnCl_3$ was prepared by the reaction of Ln_2O_3 with hydrochloric acid (5 M),[24] followed by evaporation of the solvent under reduced pressure. Infrared spectra (IR) were recorded on solid state samples using an attenuated total reflectance Perkin Elmer Spectrum 100 FT-IR. IR spectra were recorded from 4000 to 650 cm^{-1}; the intensities of the IR bands are reported as strong (s), medium (m), or weak (w), with broad (br) bands also specified. Melting points were determined using a BI Barnsted Electrothermal 9100 apparatus. Elemental analyses were obtained at either Curtin University or the University of Tasmania.

Magnetic Measurements

Magnetisation measurements were performed using a Quantum Design MPMS3 SQUID magnetometer. Temperature dependent magnetic susceptibility measurements were made on powdered polycrystalline samples suspended in eicosane for the $\{Tb_2K_2\}$, $\{Dy_2K_2\}$, $\{Ho_2K_2\}$ and $\{Gd_2K_2\}$ assemblies in an applied field of 100 Oe from 2-300 K. In addition, magnetisation curves in fields up to 7 T were measured at 2 K. Results have been corrected for the diamagnetism of the sample holder, eicosane and ligand.

General Synthesis of $[Ln(Ae{\cdot}HOR)(L)_4]_2$

To a mixture of **L**H (68-72 mg, 0.21 mmol) and hydrated $LnCl_3$ (20 mg), an aqueous AeOH solution (Ae^+ = Na^+, K^+, Rb^+; 1 M, 206-218 µL, 0.21 mmol) was added. Alcoholic solvent (EtOH; 10 ml) was added and the mixture heated at reflux for 30 minutes. The resulting mixture was hot filtered and the filtrate left to stand at RT. Slow evaporation of the solvent over several days afforded yellow crystals (10-40 mg).

$[Gd(K{\cdot}HOEt)(\mathbf{L})_4]_2$

M.p. 269-270 °C. elemental analysis calcd (%) for $C_{180}H_{132}Gd_2K_2O_{26}{\cdot}0.5(H_2O)$: C, 69.46; H, 4.31; found: C, 69.05; H, 4.05; ATR-IR: ν = 3642 w, 3567 w, 3057 w, 3027 w, 1645 m, 1609

w, 1583 s, 1543 s, 1491 m, 1447 m, 1368 s, 1311 m, 1277 m, 1178 w, 1150 m, 1073 w, 1027 w, 1013 w, 999 w, 928 w, 897 m, 823 w, 780 w, 745 m, 694 m, 668 cm^{-1} w.

*[Gd(Rb·HOEt)(**L**)$_4$]$_2$*

M.p. 263-264 °C; elemental analysis calcd (%) for $C_{180}H_{132}Gd_2Rb_2O_{26}$: C, 67.64; H, 4.16; found: C, 67.65; H, 3.51; the elemental analysis deviates somewhat from the theoretical values, possibly due to the presence of multiple solvates; ATR-IR: ν = 3650 w, 3571 w, 3057 w, 3021 w, 1645 m, 1610 w, 1584 s, 1543 s, 1491 m, 1448 m, 1369 s, 1311 m, 1278 m, 1179 w, 1151 m, 1074 w, 1027 w, 1013 w, 999 w, 925 w, 898 m, 823 w, 812 w, 780 w, 747 m, 694 m, 669 cm^{-1} w.

*[Tb(Na·HOEt)(**L**)$_4$]$_2$*

M.p. 262-263 °C. elemental analysis calcd (%) for $C_{180}H_{132}Tb_2Na_2O_{26}$: C, 70.31; H, 4.33; found: C, 69.74; H, 4.33; elemental analysis deviates somewhat from the theoretical values, possibly due to the presence of multiple solvates; ATR-IR: ν = 3644 w, 3557 w, 3058 w, 3032 w, 1645 m, 1584 s, 1543 s, 1491 m, 1448 m, 1369 s, 1311 m, 1278 m, 1179 w, 1150 m, 1073 w, 1027 w, 1013 w, 999 w, 974 w, 923 w, 898 m, 823 w, 780 w, 746 m, 694 m, 669 cm^{-1} w.

*[Tb(K·HOEt)(**L**)$_4$]$_2$*

M.p. 239-241 °C; elemental analysis calcd (%) for $C_{180}H_{132}Tb_2K_2O_{26}\cdot 1.5(H_2O)$: C, 68.98; H, 4.34; found: C, 68.50; H, 3.83; elemental analysis deviates somewhat from the theoretical values, possibly due to the presence of multiple solvates; ATR-IR: ν = 3648 w, 3567 w, 3057 w, 3024 w, 1645 m, 1609 w, 1584 s, 1542 s, 1491 m, 1448 m, 1368 s, 1311 m, 1277 m, 1179 w, 1151 m, 1073 w, 1027 w, 1013 w, 999 w, 975 w, 929 w, 897 m, 823 w, 780 w, 747 m, 694 m, 669 cm^{-1} w.

*[Tb(Rb·HOEt)(**L**)$_4$]$_2$*

M.p. 263-264 °C; elemental analysis calcd (%) for $C_{180}H_{132}Tb_2Rb_2O_{26}\cdot 3(H_2O)$: C, 66.44; H, 4.27; found: C, 66.13; H, 3.35; the elemental analysis deviates somewhat from the theoretical values, possibly due to the presence of multiple solvates; ATR-IR: ν = 3650 w, 3575 w, 3056 w, 3024 w, 1644 m, 1609 w, 1584 s, 1544 s, 1491 m, 1447 m, 1369 s, 1311 m, 1276 m, 1179 w, 1153 m, 1073 w, 1027 w, 1013 w, 999 w, 925 w, 897 m, 824 w, 780 w, 748 m, 694 m, 669 cm^{-1} w.

*[Dy(K·HOEt)(**L**)$_4$]$_2$*

M.p. 262-263 °C; elemental analysis calcd (%) for $C_{180}H_{132}Dy_2K_2O_{26}$: C, 69.42; H, 4.27; found: C, 69.60; H, 3.78; ATR-IR: ν = 3650 w, 3563 w, 3055 w, 3019 w, 2972 w, 1645 m, 1609 w, 1584 m, 1545 s, 1490 m, 1447 m, 1371 s, 1310 m, 1279 m, 1193 w, 1177 w, 1151 m, 1072 w, 1028 w, 1010 w, 975 w, 927 w, 898 m, 824 w, 780 w, 749 m, 694 m, 668 cm^{-1} w.

*[Dy(Rb·HOEt)(**L**)$_4$]$_2$*

M.p. 267-268 °C; elemental analysis calcd (%) for $C_{180}H_{132}Dy_2Rb_2O_{26}\cdot 0.5(H_2O)$: C, 67.23; H, 4.17; found: C, 66.81; H, 3.59; the elemental analysis deviates somewhat from the theoretical values, possibly due to the presence of multiple solvates; ATR-IR: ν = 3653 w, 3571 w, 3057 w, 1645 m, 1611 w, 1584 s, 1545 s, 1491 m, 1447 m, 1373 s, 1311 m, 1277 m, 1178 w, 1151 m, 1073 w, 1027 w, 1013 w, 999 w, 976 w, 925 w, 898 m, 823 w, 812w, 780 w, 748 m, 694 m, 668 cm^{-1} w.

*[Ho(K·HOEt)(**L**)$_4$]$_2$*

M.p. 260-261 °C; elemental analysis calcd (%) for $C_{180}H_{132}Ho_2K_2O_{26}$: C, 69.31; H, 4.27; found: C, 69.11; H, 3.87; ATR-IR: ν = 3567 w, 3059 w, 3019 w, 2968 w, 1668 m, 1644 m, 1611 w, 1584 s, 1546 s, 1490 m, 1447 m, 1389 s, 1371 s, 1310 m, 1279 m, 1195 w, 1180 w, 1179 w, 1151 m, 1074 w, 1024 w, 1012 w, 999 w, 927 w, 898 m, 840 w, 823 w, 778 w, 749 m, 749 w, 694 m, 668 cm^{-1} w.

*[Ho(Rb·HOEt)(**L**)$_4$]$_2$*

M.p. 268-270 °C; elemental analysis calcd (%) for $C_{180}H_{132}Ho_2Rb_2O_{26}$: C, 67.31; H, 4.14; found: C, 66.84; H, 3.68; ATR-IR: ν = 3660 w, 3570 w, 3056 w, 1645 m, 1612 w, 1584 s, 1548 s, 1492 m, 1447 m, 1373 s, 1311 m, 1278 m, 1179 w, 1151 m, 1073 w, 1027 w, 1013 w, 999 w, 976 w, 924 w, 897 m, 824 w, 780 w, 749 m, 695 m, 669 cm^{-1} w.

X-ray Crystallography

Crystallographic data for the structures were collected at 100(2) K on an Oxford Diffraction Gemini or Xcalibur diffractometer fitted with Mo Kα or Cu Kα radiation**.** Following absorption corrections and solution by direct methods, the structures were refined against F^2 with full-matrix least-squares using the program SHELXL-97 or SHELX-2014.[25] Unless stated below, anisotropic displacement parameters were employed for the non-hydrogen atoms. Except for some ethanol hydrogen atoms, all hydrogen atoms were added at calculated positions and

refined by use of a riding model with isotropic displacement parameters based on those of the parent atom. CCDC-1443572 $[Gd(K{\cdot}HOEt)(\mathbf{L})_4]_2$, CCDC-1443573 $[Gd(Rb{\cdot}HOEt)(\mathbf{L})_4]_2$, CCDC-1443574 $[Tb(Na{\cdot}HOEt)(\mathbf{L})_4]_2$, CCDC-1443575 $[Tb(K{\cdot}HOEt)(\mathbf{L})_4]_2$, CCDC-1443576 $[Tb(Rb{\cdot}HOEt)(\mathbf{L})_4]_2$, CCDC-1443577 $[Dy(K{\cdot}HOEt)(\mathbf{L})_4]_2$, CCDC-1443578 $[Dy(K{\cdot}HOEt)(\mathbf{L})_4]_2{\cdot}2EtOH$, CCDC-1443579 $[Dy(Rb{\cdot}HOEt)(\mathbf{L})_4]_2$, CCDC-1443580 $[Ho(K{\cdot}HOEt)(\mathbf{L})_4]_2$, and CCDC-1443581 $[Ho(Rb{\cdot}HOEt)(\mathbf{L})_4]_2$ contain supplementary crystallographic data, and can be obtained free of charge *via* http://www.ccdc.cam.ac.uk/conts/retrieving.html, or from the Cambridge Crystallographic Data Centre, 12 Union Road, Cambridge CB2 1EZ, U.K.; fax: (+44) 1223-336-033; or e-mail: deposit@ccdc.cam.ac.uk

X-ray data refinement

$[Gd(K{\cdot}HOEt)(\mathbf{L})_4]_2{\cdot}2EtOH$

Empirical formula $C_{184}H_{144}Gd_2K_2O_{28}$; *MW* = 3195.68. Triclinic, space group $P\bar{1}$, *a* = 13.9309(3), *b* = 14.8457(3), *c* = 19.6249(5) Å, α = 80.167(2)°, β = 72.496(2)°, γ = 90.110(2)°, Volume = 3807.77(16) $Å^3$, *Z* = 1; ρ_c = 1.394 Mg/m^3, μ = 0.993 mm^{-1}, crystal size 0.53 x 0.29 x 0.21 mm^3; $\theta_{min,\,max}$ = 2.04, 34.00°. Reflections collected = 120523, unique reflections = 31054 [*R*(int) = 0.0428]. Max. and min. transmission = 0.842 and 0.728. Number of parameters = 1087, S = 1.061; Final R indices [$I>2\sigma(I)$] *R*1 = 0.0345, *wR*2 = 0.0791; R indices (all data) *R*1 = 0.0419, *wR*2 = 0.0824; Largest diff. peak and hole 2.032 and -1.195 e. $Å^{-3}$. One phenyl ring and both the coordinated and uncoordinated ethanol solvent molecules were modelled as being disordered over two sets of sites with occupancies constrained to 0.5 after trail refinement. The coordinated ethanol OH hydrogen atoms were not located.

$[Gd(Rb{\cdot}HOEt)(\mathbf{L})_4]_2{\cdot}2EtOH$

Empirical formula $C_{184}H_{144}Gd_2Rb_2O_{28}$; *MW* = 3288.42. Triclinic, space group $P\bar{1}$, *a* = 14.0074(3), *b* = 14.8085(4), *c* = 19.7192(4) Å, α = 80.083(2)°, β = 72.374(2)°, γ = 90.044(2)°, Volume = 3833.95(16) $Å^3$, *Z* = 1; ρ_c = 1.424 Mg/m^3, μ = 1.563 mm^{-1}, crystal size 0.31 x 0.22 x 0.16 mm^3; $\theta_{min,\,max}$ = 2.80, 31.97°. Reflections collected = 47040, unique reflections = 24546 [*R*(int) = 0.0284]. Max. and min. transmission = 0.810 and 0.696. Number of parameters = 1093, S = 1.033; Final R indices [$I>2\sigma(I)$] *R*1 = 0.0366, *wR*2 = 0.0829; R indices (all data) *R*1 = 0.0453, *wR*2 = 0.0873; Largest diff. peak and hole 1.828 and -1.375 e. $Å^{-3}$. One phenyl ring and both the coordinated and uncoordinated ethanol solvent molecules were modelled as being

disordered over two sets of sites with occupancies constrained to 0.5 after trail refinement. The ethanol OH hydrogen atoms positions were refined with geometries restrained to ideal values.

*[Tb(Na·HOEt)(**L**)$_4$]$_2$*

Empirical formula $C_{180}H_{132}Tb_2Na_2O_{26}$; *MW* = 3074.68. Triclinic, space group $P\bar{1}$, *a* = 13.8911(8), *b* = 14.6303(6), *c* = 18.0785(8) Å, α = 104.868(4)°, β = 90.597(4)°, γ = 89.885(4)°, Volume = 3550.9(3) Å^3, *Z* = 1; ρ_c = 1.438 Mg/m^3, λ = 1.54178Å, μ = 5.516 mm^{-1}, crystal size 0.25 x 0.09 x 0.07 mm^3; $\theta_{min,\ max}$ = 3.13, 67.34°. Reflections collected = 34110, unique reflections = 12611 [*R*(int) = 0.0645]. Max. and min. transmission = 0.728 and 0.389. Number of parameters = 946, S = 1.030; Final R indices [*I*>2σ(*I*)] *R*1 = 0.0519, *wR*2 = 0.1267; R indices (all data) *R*1 = 0.0629, *wR*2 = 0.1366; Largest diff. peak and hole 2.023 and -0.963 e. Å^{-3}.

*[Tb(K·HOEt)(**L**)$_4$]$_2$*

Empirical formula $C_{180}H_{132}K_2O_{26}Tb_2$; *MW* = 3106.89. Triclinic, space group $P\bar{1}$, *a* = 13.9716(3), *b* = 14.5463(5), *c* = 18.1001(4) Å, α = 104.116(2)°, β = 89.996(2)°, γ = 89.797(2)°, Volume = 3582.59(17) Å^3, *Z* = 1; ρ_c = 1.440 Mg/m^3, μ = 1.114 mm^{-1}, crystal size 0.420 x 0.175 x 0.088 mm^3; $\theta_{min,\ max}$ = 2.04, 28.00°. Reflections collected = 30660, unique reflections = 17248 [*R*(int) = 0.0308]. Max. and min. transmission = 0.911 and 0.700. Number of parameters = 946, S = 1.052; Final R indices [*I*>2σ(*I*)] *R*1 = 0.0494, *wR*2 = 0.1056; R indices (all data) *R*1 = 0.0628, *wR*2 = 0.1115; Largest diff. peak and hole 2.749 and -1.660 e. Å^{-3}. The ethanol OH hydrogen atom was not located.

*[Tb(Rb·HOEt)(**L**)$_4$]$_2$·2EtOH*

Empirical formula $C_{184}H_{144}Tb_2Rb_2O_{28}$; *MW* = 3243.73. Triclinic, space group $P\bar{1}$, *a* = 13.9918(2), *b* = 14.7907(6), *c* = 19.7441(3) Å, α = 80.170(1)°, β = 72.319(1)°, γ = 90.086(1)°, Volume = 3829.65(11) Å^3, *Z* = 1; ρ_c = 1.406 Mg/m^3, μ = 1.621 mm^{-1}, crystal size 0.47 x 0.44 x 0.28 mm^3; $\theta_{min,\ max}$ = 2.14, 41.15°. Reflections collected = 160326, unique reflections = 49625 [*R*(int) = 0.0445]. Max. and min. transmission = 0.703 and 0.526. Number of parameters = 1081, S = 1.004; Final R indices [*I*>2σ(*I*)] *R*1 = 0.0355, *wR*2 = 0.0693; R indices (all data) *R*1 = 0.0502, *wR*2 = 0.0742; Largest diff. peak and hole 1.880 and -1.056 e. Å^{-3}. One phenyl ring and both the coordinated and uncoordinated ethanol solvent molecules were modelled as being disordered over two sets of sites with occupancies constrained to 0.5 after trail refinement. Hydrogen atoms on the ethanol oxygen atoms were not located.

*[Dy(K·HOEt)(**L**)$_4$]$_2$*

Empirical formula $C_{180}H_{132}Dy_2K_2O_{26}$; *MW* = 3114.06. Triclinic, space group $P\bar{1}$, *a* = 13.9658(4), *b* = 14.5111(4), *c* = 18.0746(5) Å, α = 103.049(2)°, β = 90.026(2)°, γ = 89.566(2)°, Volume = 3568.29(17) Å^3, *Z* = 1; ρ_c = 1.449 Mg/m^3, μ = 1.174 mm^{-1}, crystal size 0.24 x 0.21 x 0.10 mm^3; $\theta_{min,\ max}$ = 2.83, 30.00°. Reflections collected = 85194, unique reflections = 20748 [*R*(int) = 0.0582]. Max. and min. transmission = 0.895 and 0.823. Number of parameters = 947, S = 1.157; Final R indices [*I*>2σ(*I*)] *R*1 = 0.0701, *wR*2 = 0.1635; R indices (all data) *R*1 = 0.0807, *wR*2 = 0.1681; Largest diff. peak and hole 4.190 and -1.589 e. Å^{-3}. The ethanol OH hydrogen atom was not located.

*[Dy(K·HOEt)(**L**)$_4$]$_2$·2EtOH*

Empirical formula $C_{184}H_{144}Dy_2K_2O_{28}$; *MW* = 3206.19. Triclinic, space group $P\bar{1}$, *a* = 13.9132(5), *b* = 14.8410(8), *c* = 19.6256(8) Å, α = 80.221(4)°, β = 72.392(4)°, γ = 89.987(4)°, Volume = 3800.8(3) Å^3, *Z* = 1; ρ_c = 1.401 Mg/m^3, μ = 1.105 mm^{-1}, crystal size 0.21 x 0.11 x 0.04 mm^3; $\theta_{min,\ max}$ = 2.79, 27.00°. Reflections collected = 27980, unique reflections = 16193 [*R*(int) = 0.0374]. Max. and min. transmission = 0.959 and 0.764. Number of parameters = 1081, S = 0.993; Final R indices [*I*>2σ(*I*)] *R*1 = 0.0417, *wR*2 = 0.0861; R indices (all data) *R*1 = 0.0529, *wR*2 = 0.0908; Largest diff. peak and hole 0.992 and -1.054 e. Å^{-3}. One phenyl ring and both the coordinated and uncoordinated ethanol solvent molecules were modelled as being disordered over two sets of sites with occupancies constrained to 0.5 after trail refinement. The ethanol OH hydrogen atoms were not located.

*[Dy(Rb·HOEt)(**L**)$_4$]$_2$·2EtOH*

Empirical formula $C_{184}H_{144}Dy_2Rb_2O_{28}$; *MW* = 3298.93. Triclinic, space group $P\bar{1}$, *a* = 13.9581(3), *b* = 14.7899(3), *c* = 19.7191(3) Å, α = 80.097(2)°, β = 72.276(2)°, γ = 90.065(2)°, Volume = 3813.58(13) Å^3, *Z* = 1; ρ_c = 1.436 Mg/m^3, μ = 1.681 mm^{-1}, crystal size 0.28 x 0.19 x 0.11 mm^3; $\theta_{min,\ max}$ = 2.80, 35.94°. Reflections collected = 113525, unique reflections = 34619 [*R*(int) = 0.0619]. Max. and min. transmission = 0.868 and 0.722. Number of parameters = 1081, S = 1.092; Final R indices [*I*>2σ(*I*)] *R*1 = 0.0537, *wR*2 = 0.1071; R indices (all data) *R*1 = 0.0703, *wR*2 = 0.1136; Largest diff. peak and hole 3.134 and -1.253 e. Å^{-3}. One phenyl ring and both the coordinated and uncoordinated ethanol solvent molecules were modelled as being disordered over two sets of sites. The ethanol OH hydrogen atoms were not located.

*[Ho(K·HOEt)(**L**)$_4$]$_2$*

Empirical formula $C_{180}H_{132}Ho_2K_2O_{26}$; *MW* = 3118.92. Triclinic, space group $P\bar{1}$, *a* = 14.0116(4), *b* = 14.5056(3), *c* = 18.0275(4) Å, α = 102.746(2)°, β = 90.006(2)°, γ = 89.190(2)°, Volume = 3573.36(15) Å^3, *Z* = 1; ρ_c = 1.449 Mg/m^3, μ = 1.234 mm^{-1}, crystal size 0.59 x 0.43 x 0.19 mm^3; $\theta_{min,\ max}$ = 2.84, 30.00°. Reflections collected = 96102, unique reflections = 20828 [*R*(int) = 0.0415]. Max. and min. transmission = 0.799 and 0.588. Number of parameters = 946, S = 1.063; Final R indices [$I>2\sigma(I)$] *R*1 = 0.0354, *wR*2 = 0.0878; R indices (all data) *R*1 = 0.0392, *wR*2 = 0.0904; Largest diff. peak and hole 2.303 and -1.233 e. Å^{-3}. The ethanol OH hydrogen atom was not located with sufficient confidenceto be included in the model.

*[Ho(Rb·HOEt)(**L**)$_4$]$_2$·2EtOH*

Empirical formula $C_{184}H_{144}Ho_2Rb_2O_{28}$; *MW* = 3303.79. Triclinic, space group $P\bar{1}$, *a* = 13.9449(8), *b* = 14.7815(6), *c* = 19.7069(11) Å, α = 80.013(4)°, β = 72.296(5)°, γ = 90.008(4)°, Volume = 3805.0(3) Å^3, *Z* = 1; ρ_c = 1.442 Mg/m^3, μ = 1.743 mm^{-1}, crystal size 0.21 x 0.09 x 0.045 mm^3; $\theta_{min,\ max}$ = 2.14, 28.34°. Reflections collected = 28503, unique reflections = 16616 [*R*(int) = 0.0493]. Max. and min. transmission = 0.963 and 0.855. Number of parameters = 1021, S = 1.023; Final R indices [$I>2\sigma(I)$] *R*1 = 0.0528, *wR*2 = 0.0811; R indices (all data) *R*1 = 0.0767, *wR*2 = 0.0891; Largest diff. peak and hole 1.027 and -0.924 e. Å^{-3}. One phenyl ring, and both the coordinated and uncoordinated ethanol solvent molecules were modelled as being disordered over two sets of sites with occupancies constrained to 0.5 after trail refinement. Disordered atoms were refined with isotropic displacement parameters. Hydrogen atoms on the ethanol oxygen atoms were not located.

Acknowledgments

M.M. wishes to thank the ARC for funding (FT1301000033). B.L.R. wishes to thank Curtin University for the Australian Postgraduate Award. The authors acknowledge access to the facilities at the Centre for Microscopy, Characterisation and Analysis, University of Western Australia.

Supporting Information

The Supporting information contains molecular displacement plots of all assemblies not presented herein, and raw Ln-O distances for all crystal structures.

References

[1] J.-C. G. Bünzli, *Coord. Chem. Rev.* **2015**, *293-294*, 19–47.

[2] M. A. Katkova, M. N. Bochkarev, *Dalt. Trans.* **2010**, *39*, 6599–6612.

[3] J.-C. G. Bünzli, *Acc. Chem. Res.* **2006**, *39*, 53–61.

[4] J.-C. G. Bünzli, S. V. Eliseeva, *J. Rare Earth.* **2010**, *28*, 824–842.

[5] S. V. Eliseeva, J.-C. G. Bünzli, *New J. Chem.* **2011**, *35*, 1165–1176.

[6] R. Sessoli, A. K. Powell, *Coord. Chem. Rev.* **2009**, *253*, 2328–2341.

[7] S. Faulkner, S. J. A. Pope, B. P. Burton-Pye, *Appl. Spectrosc. Rev.* **2005**, *40*, 1–31.

[8] J.-C. G. Bünzli, *J. Lumin.* **2015**, 1–13.

[9] P. C. Andrews, W. J. Gee, P. C. Junk, M. Massi, *New J. Chem.* **2013**, *37*, 35–48.

[10] K. Binnemans, in *Handb. Phys. Chem. Rare Earths* (Eds.: K.A. Gschneidner, J.-C.G. Bunzli, V.J. Pecharsky), Elsevier B.V., Amsterdam, The Netherlands, **2005**, pp. 107–272.

[11] D. T. Thielemann, A. T. Wagner, Y. Lan, P. Oña-Burgos, I. Fernández, E. S. Rösch, D. K. Kölmel, A. K. Powell, S. Bräse, P. W. Roesky, *Chem. Eur. J.* **2015**, *21*, 2813–2820.

[12] D. T. Thielemann, A. T. Wagner, E. Rösch, D. K. Kölmel, J. G. Heck, B. Rudat, M. Neumaier, C. Feldmann, U. Schepers, S. Bräse, et al., *J. Am. Chem. Soc.* **2013**, *135*, 7454–7457.

[13] M. Ismail, S. J. Lyle, J. E. Newbery, *J. Inorg. Nucl. Chem.* **1969**, *31*, 2091–2093.

[14] G. A. Crosby, R. E. Whan, *J. Chem. Phys.* **1960**, *32*, 614–615.

[15] G. A. Crosby, R. E. Whan, R. M. Alire, *J. Chem. Phys.* **1961**, *34*, 743–748.

[16] B. L. Reid, S. Stagni, J. M. Malicka, M. Cocchi, G. S. Hanan, M. I. Ogden, M. Massi, *Chem. Commun.* **2014**, *50*, 11580–11582.

[17] B. L. Reid, S. Stagni, J. M. Malicka, M. Cocchi, A. N. Sobolev, B. W. Skelton, E. G. Moore, G. S. Hanan, M. I. Ogden, M. Massi, *Chem. - A Eur. J.* **2015**, *21*, 18354–18363.

[18] S. Demir, J. M. Zadrozny, M. Nippe, J. R. Long, *J. Am. Chem. Soc.* **2012**, *134*, 18546–18549.

[19] J. D. Rinehart, M. Fang, W. J. Evans, J. R. Long, *Nat. Chem.* **2011**, *3*, 538–542.

[20] M. Llunell, D. Casanova, J. Cirera, P. Alemany, S. Alvarez, "Shape version 2.1," can be found under <http://www.ee.ub.es/index.php/news-ee/575-shape-available>, **2013**.

[21] D. Casanova, M. Llunell, P. Alemany, S. Alvarez, *Chem. Eur. J.* **2005**, *11*, 1479–1494.

[22] J. Tang, I. Hewitt, N. T. Madhu, G. Chastanet, W. Wernsdorfer, C. E. Anson, C. Benelli, R. Sessoli, A. K. Powell, *Angew. Chemie Int. Ed.* **2006**, *45*, 1729–1733.

[23] M. L. Kahn, J.-P. Sutter, S. Golhen, P. Guionneau, L. Ouahab, O. Kahn, D. Chasseau, *J. Am. Chem. Soc.* **2000**, *122*, 3413–3421.

[24] V. S. Sastri, J.-C. G. Bünzli, V. R. Rao, G. V. S. Rayudu, J. R. Perumareddi, in *Mod. Asp. Rare Earths Their Complexes*, Elsevier, **2003**, pp. 259–374.

[25] G. M. Sheldrick, *Acta Crystallogr. Sect. C-Struct. Chem.* **2015**, *71*, 3–8.